Planning Safe Flight Routes for Urban Air Mobility using Ground Risk Maps

Jan Kleikemper[1] and Ludwig Kempf[1]

[1]Institute of Flight Systems and Automatic Control, Technical University of Darmstadt
kleikemper@fsr.tu-darmstadt.de

Abstract

New aircraft categories like electric take-off and landing aircraft (eVTOL) are being developed to enable flight operations in the context of Urban Air Mobility (UAM). However, eVTOL operations in urban airspace pose new challenges, particularly with regard to the ground risk and significant damage resulting from crashes. This paper proposes a new methodology for quantifying the direct risk of eVTOL flights to uninvolved people on the ground. Probabilistic grid-based maps are calculated, where each grid cell represents the ground risk resulting from flying over that cell. The risk is estimated by applying Monte Carlo Simulations for three different types of descent trajectories. New models for the probabilities of critical eVTOL failures and collisions with buildings, a dynamic population distribution, and a new approach to modeling impact damage are presented. The proposed approach uses only open access and globally available geographical data. An exemplary examination of the generated ground risk maps reveals significant risk values especially over densely populated cities which underlines the relevance of incorporating ground risk considerations in the operational concepts of UAM. Possible applications of the ground risk maps for path planning problems are shown. The results demonstrate how using ground risk maps can contribute to enabling safe and efficient UAM operations. This could support the development of necessary regulations for eVTOL operations above populated areas.

1 Introduction

Operations of small Unmanned Aircraft Systems (sUAS) in the urban airspace for different purposes like surveillance, inspection and light-weight cargo transport have been subject to research for over a decade [9]. However, a large rise of operations has not happened, yet, due to a variety of reasons including missing regulations [5]. Recently, the concept of Urban Air Mobility (UAM) has gained increasing attention [28]. The core idea behind UAM is the transport of people and heavy cargo through the urban airspace using eVTOLs [8]. The advantage is saving time due to bypassing of traffic in metropolitan areas [30]. As is the case for sUAS operations, UAM operations will take place in low airspaces over densely populated areas, entailing that crashes would harm uninvolved people on the ground. eVTOL operations are characterised by higher masses, velocities and altitudes than sUAS operations which increases the potential harm resulting from crashes and increases the urgency to assess and mitigate their ground risk.
Currently, flight operations in urban airspace are highly restricted. A recent social study conducted by the European Union Aviation Safety Agency (EASA) about the perception of future UAM operations revealed, that besides additional noise pollution, most people are concerned about their safety [6]. This underlines the necessity for new, well-balanced regulations enabling the UAM operations while maintaining safety standards. Quantifying the risk will enable an informed decision making with regard to safe UAM operations.

1.1 Related work

Extensive research in support of risk assessments for UAM operations has been conducted in the past. Based on a study of UAM mission requirements [17], Silva et al. have developed three concepts of eVTOLs with detailed specifications [24]. Several publications exist on the risk assessment for sUAS (operating in urban environments), which are also applicable for the introduction of eVTOLs. Lum and Waggoner provide a risk model for UAS

operations that covers midair collisions and ground strikes, including operations over densely populated areas [14]. Finally, a risk assessment process for sUAS that incorporates different descent types, vehicle characteristics, geospatial data and respective uncertainties is provided by La Cour-Harbo [12, 13]. Primatesta et al. build on this work to provide a framework for generating probabilistic ground risk maps (GRM) and risk-minimizing path planning for sUAS in urban airspace [20]. An approach to risk-minimizing path planning for UAM is provided by Sláma et al. [25]. They add a safe emergency landing condition, which improves the overall risk that is inherent to a flight operation. Wu et al. introduce a risk domain formulation for path planning of eVTOLs that incorporates static and dynamic obstacles and uncertainties about obstacle and vehicle properties [32].

1.2 Research gap

The risk map framework by Primatesta et al. has been developed for sUAS. However, eVTOLs will operate with a higher mass and mission altitude. Both are sensitive inputs of the risk assessment, as the mass defines the kinetic energy of the impact (and therefore the risk) and the altitude sets the radius of the possible impact zone. This paper aims to adapt the existing risk assessment framework to account for the demanding boundary conditions of UAM operations. Besides introducing modified vehicle specifications of eVTOLs, a new impact modeling and the use of geospatial data are proposed to enable an in-depth risk assessment of UAM operations. Specifically, a dynamic population model, a more precise prediction of the impact location in densely built-up areas and a detailed modeling of the dissipation of kinetic energy upon impact with buildings are provided, thus increasing the accuracy of the risk assessment.
The remainder of this paper is structured as follows. The methodology for the ground risk map is outlined in Section 2. Section 3 gives a detailed description of the models. The resulting GRMs are applied to calculate minimum risk paths in Section 4. Subsequently, the methodology and results are discussed in Section 5 and the paper concludes with a summary and statement of open questions in Section 6.

2 Ground Risk Map Methodology

The probability of a fatality caused by an eVTOL crash is composed of three partial probabilities: 1) the probability of an uncontrolled eVTOL descent, 2) the probability of the descending eVTOL impacting people on the ground and 3) the probability of the impact being fatal [20]. The probability of an uncontrolled descent event is governed by the failure rates of the eVTOL. Monte Carlo Simulations (MCS) are used to predict the descent trajectories following a failure. Linearizing the descent trajectories allows to predict whether a descending eVTOL hits an obstacle or the ground. The fatality value is finally calculated by determining the exposed geometry and the number of impacted people. The following Section 3 introduces an attempt to model these partial probabilities. As a whole, they form the risk assessment that is used to calculate the final GRMs later on. Figure 1 illustrates the steps and connections of the risk assessment.

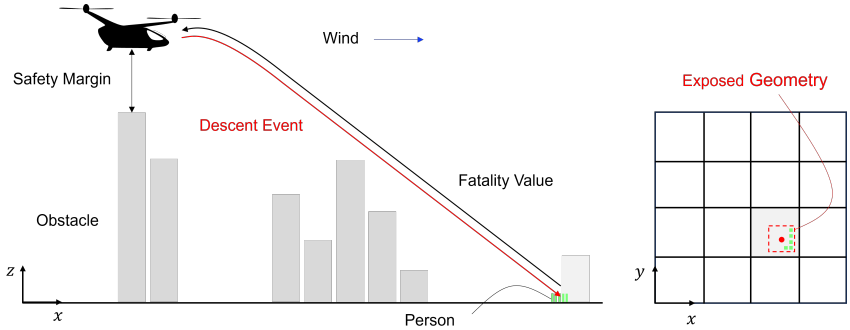

Figure 1: Elements and connections of the risk map methodology, example of one grid cell. The impact point depends on the type of descent event, wind and potential obstacles. The fatality value is influenced by the exposed geometry and the number of people in the impacted cell.

3 Models

Several computational models are required for the subsequent implementation of the risk map generation. It is essential to consider the reliability of the eVTOL carrying out the flight mission. Furthermore, the extent of the exposed geometry during the impact, the number of people involved in the crash, and the characteristics of the impact event must be quantified.

3.1 Aircraft failure model

The first step in the risk assessment is to predict the probability of an uncontrolled eVTOL descent. Different architecture configurations of eVTOLs were proposed in the past. To assure applicability of the risk map methodology independent from developments in the general aircraft architecture, three different eVTOL design classes are used in this work: Side-by-side helicopter (SbS), Quadrotor (Quad) and Lift+cruise eVTOL (L+C). They are based on the NASA Design and Analysis of Rotorcraft (NDARC) tool and chosen to represent a majority of possible architectures [24]. Key properties for each eVTOL design class that will be used in the calculations later on are summarised in Table 1.

Table 1: Key properties of the three different eVTOL design classes

eVTOL design class	**SbS**	**Quad**	**L+C**
Number of engines [-]	2	4	8
Mass m_v [kg]	2220	2940	3720
Fuselage cross section A_v [m^2]	2.5	4	2.5
Length l_v [m]	8.5	11	8
Wingspan b_v [m]	10	12	11
Glide ratio E [-]	N(7.2,1)	N(5.8,1)	N(8.5,1)
Fuselage drag C_f [-]	N(1.6,0.2)	N(1.4,0.2)	N(1.7,0.2)
Parachute deployment delay t_d [s]	10	12	15
Canopy area A_c [m^2]	320	430	540
Parachute drag C_p [-]	N(1.3,0.2)	N(1.3,0.2)	N(1.3,0.2)

All three eVTOL design classes used in this work rely on thrust from rotors for stable flight. In absence of historical data, the failure rates of eVTOLs are based on the number of engines each eVTOL has. A critical engine configuration that would lead to a critical loss of thrust and thus loss of control (LOC) is defined for each eVTOL design class. The probability of eVTOL failure and therefore uncontrolled descent is then a superposition of probabilities of single engine failures. Statistics on helicopter accidents report 3.5×10^{-6} fatalities per flight hour for twin-engine helicopters which is only $53\,\%$ of the number stated for single-engine helicopters accidents [15]. This leads to the conclusion that a redundancy of three engines could reduce the failure rate by at least another $53\,\%$. By assuming that each rotor has its own engine and applying the helicopter statistics to the three eVTOL design classes, it is possible to assign an overall failure rate to each class based on the ability to maintain stability after losing a certain number of engines. The SbS will descend after losing one engine, while the Quad will destabilize after losing two engines [16]. Finally, the L+C will experience a LOC for three affected engines. Figure 2 showcases the critical engine failure combinations for the three eVTOL design classes.

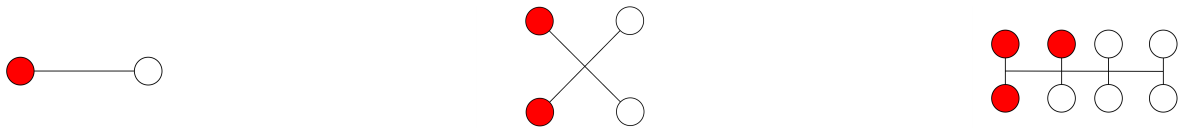

(a) SbS (b) Quad (c) L+C

Figure 2: Overview of the critical engine failure combinations. The minimum affected engines leading to an eVTOL failure are highlighted in red.

As a consequence of the LOC, the eVTOL will crash uncontrollably into the ground. Depending on the cause for the LOC (and a variety of other factors), a crashing eVTOL can follow different descent trajectories. As in the framework by Primatesta et al., three different types of descent trajectories are considered in this work: ballistic descent, uncontrolled glide and parachute descent [20]. Each descent trajectory has different characteristics which

influence the impact position, angle and energy. As these values are important values in the risk assessment, the consideration of different descent trajectories is necessary. The impact points resulting from the descent trajectories are determined by many input values most of which are affected by uncertainties [20]. To account for these uncertainties, this work assumes a normal distribution of the relevant values. A set of possible impact impact points is then calculated using MCSs. The results of the MCSs are summarised as Probability Density Functions (PDFs) (see Figure 5a). Note, that wind influence is modeled as a linear shift according to a normally distributed wind speed and direction. The characteristic trajectories as modeled by La Cour-Harbo for each descent types are visualized in Figure 3 [13].

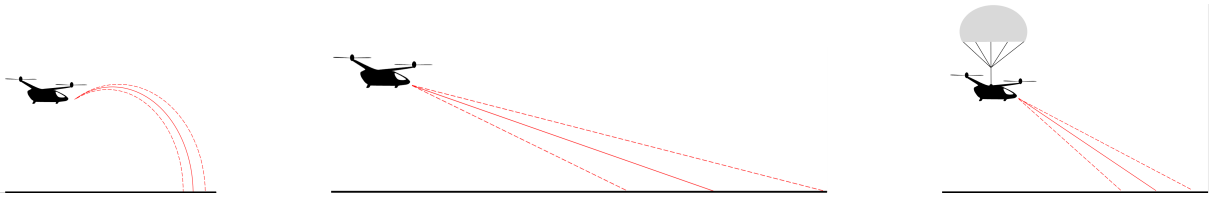

(a) Ballistic Descent (b) Uncontrolled Glide (c) Parachute Descent

Figure 3: Qualitative sketch of the three uncertainty-afflicted descent trajectory types: ballistic descent, uncontrolled glide, parachute glide. The dashed lines indicate that the impact location is uncertain.

47 % of helicopter accidents are caused by a LOC [15]. In the following, it is assumed that all LOC events lead to uncontrolled glide while any other failure cause will lead to a ballistic descent. Additionally, the usage of parachutes is considered as they can significantly reduce the impact velocity and therefore prevent fatalities on-board and on the ground. A typical state-of-the-art parachute has a successful deployment rate of 84 % [2]. In consequence, the vast majority of descents are parachute descents, with only 16 % remaining uncontrolled glides or ballistic descents. The event probabilities are listed in Table 2 for vehicles with and without parachute system (PS).

Table 2: Descent event probabilities for all three eVTOL design classes. The probabilities are different for configurations with and without parachute system (PS).

eVTOL design class	**SbS E**	**Quad E**	**L+C E**	**SbS E PS**	**Quad E PS**	**L+C E PS**
Total events	$6.6{\cdot}10^{-6}$	$3.5{\cdot}10^{-6}$	$1.9{\cdot}10^{-6}$	$6.6{\cdot}10^{-6}$	$3.5{\cdot}10^{-6}$	$1.9{\cdot}10^{-6}$
Ballistic descent	$3.5{\cdot}10^{-6}$	$1.9{\cdot}10^{-6}$	$1{\cdot}10^{-6}$	$5.6{\cdot}10^{-7}$	$3{\cdot}10^{-7}$	$1.6{\cdot}10^{-7}$
Uncontrolled glide	$3.1{\cdot}10^{-6}$	$1.6{\cdot}10^{-6}$	$0.9{\cdot}10^{-6}$	$5{\cdot}10^{-7}$	$2.6{\cdot}10^{-7}$	$1.4{\cdot}10^{-7}$
Parachute descent	-	-	-	$5.5{\cdot}10^{-6}$	$2.9{\cdot}10^{-6}$	$1.6{\cdot}10^{-6}$

3.2 Impact location

Descending eVTOLs can collide with built-up structures that are not in the cell of the predicted ground impact. This is more likely, the smaller the impact angle is (uncontrolled glide). To capture this possibility in the impact model, the impact location is predicted by detecting intersections of the linearized descent trajectory with the average building height in the potentially affected grid cells. A collision with an obstacle before hitting the ground is referred to as early impact in the following . Linearization leads to an approximation error for ballistic descent which is considered acceptable because ballistic descents are typically very steep. The probability of an early impact is determined by the ratio of built-up surface b_i to empty surface e_j in that cell. The required data about the built-up surface is taken from the Global Human Settlement Layer (GHSL) which is provided by the European Commission's Copernicus Programme [19]. The data set is based on a concept by Pesaresi et al. [18]. The pixel-based data of the GHSL is freely available for the whole globe. It is distributed in grid cells of 100 m x 100 m in the area-true Mollweide projection (ESRI:54009). An explanation of the Mollweide projection is provided by Snyder [26]. Early impacts must also be calculated in the Mollweide projection due to the angular distortion of the descent trajectory. To avoid remapping errors of the geospatial data, this work follows the methodology of a computation in the Mollweide grid. At the end of the risk assessment, the spatial classification of the risk and the waypoints of the minimum risk path will be transformed to the World Geodetic System 1984 (WGS 84).
If an early impact is predicted, cell values of the PDF and impact angle and energy are shifted to the cell of the early impact. If no early impact is predicted for the first candidate cell, all subsequent candidate cells are checked

until an early impact is predicted or the eVTOL hits the ground. All possible outcomes are summed up to receive the final PDFs as defined in Equations 1 and 2.

$$PDF_{\text{outside}} = \prod_{j=l}^{k} e_j \cdot PDF_k, \tag{1}$$

$$PDF_{\text{inside}} = \sum_{i=l}^{k} b_i \prod_{j=l}^{i-1} e_j \cdot PDF_k. \tag{2}$$

Note that by nature, the sum of all cells in both PDF arrays is always 1. The concept of early impact prediction is visualised in Figure 4. Figure 5 shows the different PDFs of impact points for the cases of unobstructed descend and adjusted descent through early impact with built-up structures.

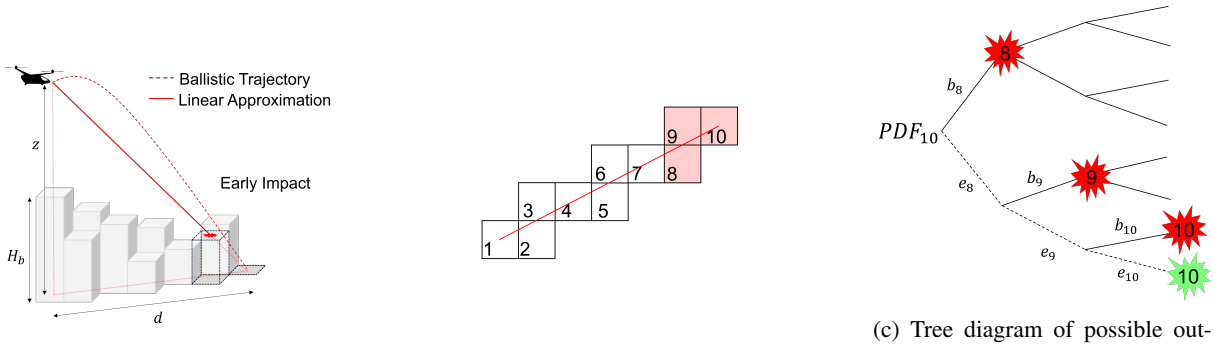

(a) Early impact (b) Affected cells (c) Tree diagram of possible outcomes

Figure 4: Representation how the early impact of descending eVTOLs with buildings is calculated by linearly approximating the descent trajectory and detecting intersections with built-up structures

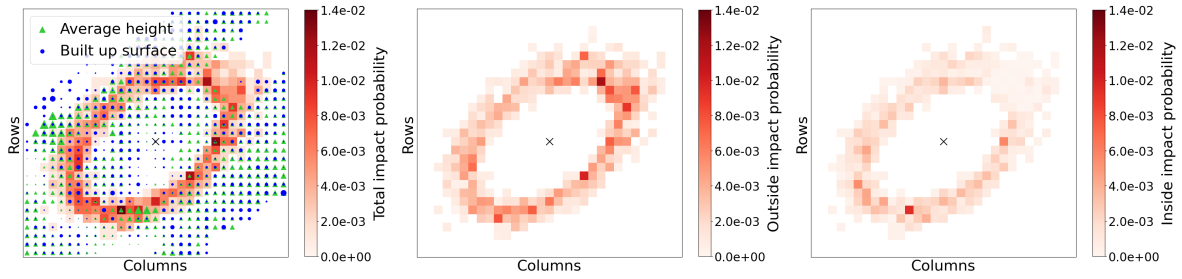

(a) Unobstructed descent (b) Outside impacts (Obstructed) (c) Inside impacts (Obstructed)

Figure 5: PDFs of impacts for unobstructed and obstructed descents in a scenario around Times Square, New York City.

3.3 Impact severity

The amount of fatalities caused by a crash are determined by the number of people that are present in the vicinity of the impact point and by the magnitude of the kinetic energy that hits the impacted people. Modelling these two values enables assessing the consequences of a crash.

3.3.1 Population distribution

The first corner stone of modelling the impact severity is the population distribution model. The more people potentially affected by the eVTOL impact, the higher the risk. The baseline residential population distribution is derived from the grid-based population map provided by the GHSL. The available population dataset by Schiavina et al. [22] is based on a concept from Freire et al. [7]. Due to migration patterns, the number of people in a location and the share of people in- and outside of buildings fluctuate throughout a day and change for different days which

is why a dynamic population model is introduced. The basic idea is to use the residential population distribution and alter it based on assumptions for the flow of intra-city commuters, in- and outcoming commuters and incoming tourists. The population flows are based on observations and assumptions for the city of Frankfurt, Germany. As this city has relatively seen the highest commuter share of all German cities, the result is deemed a conservative estimation of population numbers during work times which is particularly critical [27]. Different manifestations of the population flow are assumed for weekdays, Saturdays and Sundays. Information on commuter flow (intra-city and in-/outgoing) and incoming tourists are taken from reports [27, 29]. The number of incoming tourists is assumed to be even for each week in a year. Within a week, a 25 % increase of tourists on weekends is assumed. At the same time, commuter traffic (in- and outgoing) is assumed to decrease by 75 %, respectively 90 % on Saturdays and Sundays compared to a weekday. The exact distribution is reported in Table 3.

Table 3: Commuter and tourist flow of Frankfurt am Main

Type	Reference population	Weekday (%)	Saturday (%)	Sunday (%)
Intra-commuter	716 277 (June 2015)	36.4	9.1	3.6
Outgoing commuter	716 277 (June 2015)	14.4	3.6	1.4
Incoming commuter	716 277 (June 2015)	16.5	4.1	1.7
Tourist	764 474 (June 2022)	2.9	3.6	3.6

As buildings can offer significant shelter that reduces the impact severity it makes a large difference whether people are out- or inside of buildings during the crash. Based on a model from the National Human Activity Pattern Survey (NHAPS), the population is allocated by the hour to one group being inside buildings and another group outside (including also people inside vehicles) [11]. To now account for the population flow of each group during the day, redistributions are performed. The redistribution relies on the general land use categories residential (RES) and non-residential (NRES) which are also obtained from the GHSL [19].
Commuters leaving their domicile are subtracted from the residential population inside, while commuters and tourists coming into the city are distributed based on the non-residential volume of each cell. Regarding the population outside, commuters leaving their domicile are subtracted from the residential population outside. Every surface consisting at least of 10 % of NRES built-up surface and not more than 70 % of RES built-up surface is considered part of the total exterior surface where commuters could be present. The complete number of incoming commuters outside is redistributed by the portion of empty surface within the assigned cell compared to the total commuter surface. Every surface consisting of a maximum of 90 % of RES built-up surface is considered part of the total exterior surface where tourists could be present. Every tourist outside is redistributed by considering the portion of surface within the assigned cell compared to the total tourist surface. Figure 6 illustrates the different distributions of the population inside and outside during day time (09:00) and night time (03:00).

3.3.2 Exposed geometry

When the impact location of the descending eVTOL is determined, the consequence of impact depends on the exact exposition of the people to the aircraft in this location. The main concept for the exposed area is based on the work by Lum and Waggoner [14]. Their approach is to calculate an exposed surface area of the impacted people using Equation 3.

$$A_{\text{exp}} = (b_v + 2R_p)\left(l_v + \frac{H_p}{\tan\gamma} + 2R_p\right). \tag{3}$$

Wingspan b_v and length l_v are vehicle dimensions (see Section 3.1), while H_p and R_p are the person's height and radius. The size of the human body is in this work defined as the 95th percentile of a male body in Germany (conservative approach), which is a height of $H_\text{p} = 1.86\,\text{m}$ and a radius of $R_\text{p} = 0.26\,\text{m}$ [4]. The concept of the exposed surface area is only applied to the outside population in this work. The extend of the impact on the population inside is modelled using the exposed volume of built-up structures. If a grid cell is predominantly composed of built-up surface, it is assumed that descending eVTOLs will crash into a roof of the building. Otherwise, it is assumed that the impact point will be on the side of a building. The impact direction can be modeled by weighting the impact type according to the relative portion of the built-up surface. This differentiation impacts the exposed volume. It is assumed that an eVTOL will penetrate the building to a depth equal to twice its length at maximum. In correspondence with Equation 3, the exposed volume during the impact is derived from the geometry of the eVTOL and the human body. Figure 7 shows the geometry of the exposed volumes for side and top impact. Equations 4 and 5 capture the calculation of the volumes.

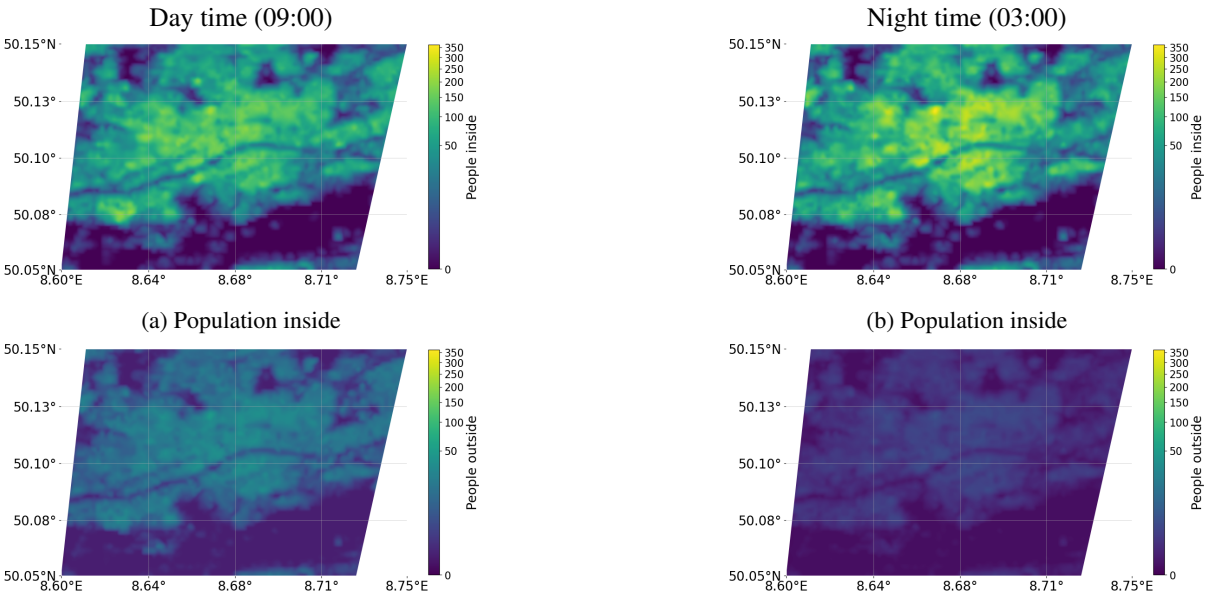

(a) Population inside

(b) Population inside

(c) Population outside

(d) Population outside

Figure 6: Population distribution of Frankfurt, separated by in- and outside population. Comparison of day and night time distribution.

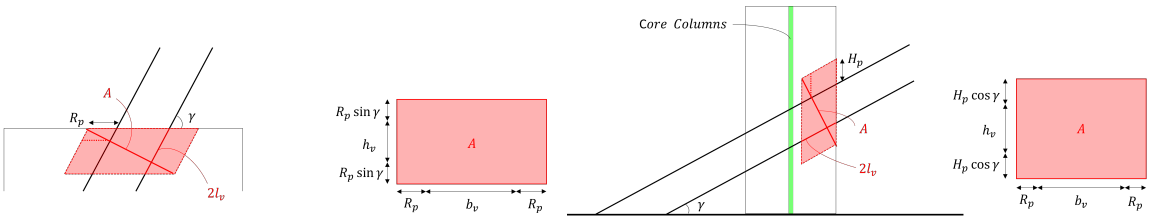

(a) Top impact

(b) Side impact.

Figure 7: The exposed volume during impact inside. Top impacts are assumed to happen, if the grid cell predominantly consists of built-up structure.

$$V_{\text{exp, side}} = 2l_v(h_v + 2H_p\cos\gamma)(b_v + 2R_p) \tag{4}$$

$$V_{\text{exp, top}} = 2l_v(h_v + 2R_p\sin\gamma)(b_v + 2R_p) \tag{5}$$

3.3.3 Impact characteristics

The severity of the impact and subsequently the potential to harm people depends on the kinetic energy of the aircraft. During the crash into a building, some of the original kinetic energy of the crashing eVTOL is dissipated by the building's structural material. The dissipated kinetic energy must be estimated to decide about the lethality of the remaining kinetic energy. The energy dissipation is calculated based on an investigation by Wierzbicki et al. of the structural mechanics involved in the collapse of the World Trade Center 2001 [31], but with simplifications due to the smaller size of eVTOLs compared to commercial airliners. Further, all buildings are assumed to be constructed of steel I-beams, which are very commonly used. The dimensions of the I-beam are defined by its height h, flange width b, flange thickness t and the web thickness s. Due to the dimensions of an eVTOL compared to a building, it is assumed that energy is dissipated during impact only through the crushing of the fuselage and the cutting through the shell of the building. This is a conservative approach. The residual energy is defined by

$$E_{\text{residual}} = E_{\text{kinetic}} - E_{\text{crush}} - E_{\text{cut}}. \tag{6}$$

Following an approach by Riera et al. [21] the crushing energy E_{crush} and he cutting energy E_{cut} are calculated by Equations 7 and 8.

$$E_{\text{crush}} = S \cdot F_{\text{crush}} \cdot l_{\text{f}}. \tag{7}$$

$$E_{\text{cut}} = \frac{\sigma_{\text{b}}}{\sqrt{3}} \cdot (2tb^2 + s^2(h - 2t)) \tag{8}$$

As the shape of an eVTOL is simplified as a cylindrical shape, S is a safety factor that accounts for deviations of the fuselage form from a perfect cylindrical shape. l_{f} is the equivalent length of the cylindrical fuselage model (set to 50 % of the eVTOL length l_v) and F_{crush} is the crushing force. Further details of the impact energy modelling can be found in the work by Riera et al. [21].
The residual energy E_{residual} needs to be evaluated for its potential to be lethal. This is done using the *Abbreviate Injury Scale* (AIS) [13] which is estimated by

$$AIS = 1.33 \cdot BC + 0.6. \tag{9}$$

In Equation 9, BC is the *Blunt Criterion* which is developed by Clare et al [3]. It is also used by Primatesta et al. in the risk assessment for sUAS [20]. The BC is defined as

$$BC = ln \frac{E_{\text{residual}}}{m_p^{1/3} t_p D}, \tag{10}$$

where t_{p} is the thickness of the body wall, m_{p} the mass of the impacted person and D the diameter of the impacting object. t_{p} is calculated by

$$t_p = \kappa \cdot m_p^{1/3} \tag{11}$$

A value of κ = 0.7 is used for males and κ = 0.6 for females. The AIS score is connected to a scale of injury severance presented in Table 4. In this work, all injuries of score 3 (serious injury) and higher are considered to be fatal as a conservative approach.

Table 4: The Abbreviate Injury Scale (AIS)

AIS score	1	2	3	4	5	6
Degree of injury	Minor	Moderate	Serious	Severe	Critical	Unsurvivable

3.4 Fatality model

To obtain the final risk value for each cell within the map frame, the impact probabilities must be calculated from the PDFs, and the fatality probabilities must be determined from the impact probabilities. The calculations are performed separately for the three types of descent events, and the final risk is then accumulated. The risk value resulting from all possible impact locations with respect to the starting point in the original cell is then returned to the origin. The ground risk is obtained by performing operations on each cell of the PDFs that are not equal to zero. The probability of impact is divided into impacts inside and outisde. The probability values $P_{\text{impact, outside}}$ and $P_{\text{impact, inside}}$ are calculated as follows:

$$P_{\text{impact, outside}} = PDF_{\text{outside}} \cdot \frac{POP_{\text{outside}}}{A_{\text{cell}} - A_b} \cdot A_{\text{exp}} \tag{12}$$

$$P_{\text{impact, inside}} = PDF_{\text{inside}} \cdot \frac{POP_{\text{inside}}}{V_b} \cdot V_{\text{exp}} \tag{13}$$

POP_{outside} and POP_{inside} are the number of people per cell and A_{cell} is its area (100 m x 100 m). A_b represents the built-up surface area within the cell and V_b is the built-up volume. Similar to the impact probability, the probability of fatality is divided into fatalities inside and outside, since the kinetic energy of the impact will change in respect of the scenario, but the calculation procedure is identical. In order to determine whether an impact leads to a fatality or not, the residual energy with impact is mapped to the AIS score and compared against a threshold value AIS_{max}. If the threshold is exceeded, the probability of fatality equals the probability of impact:

$$P_{\text{fatality, inside/outside}} = \begin{cases} P_{\text{impact, inside/outside}}, & AIS_{\text{inside/outside}} \geq AIS_{\text{max}} \\ 0, & AIS_{\text{inside/outside}} < AIS_{\text{max}} \end{cases} \tag{14}$$

Finally, the accumulated risk value that is returned to the cell where the failure originally occurred is given by Equation 15. Considering ballistic descent, uncontrolled glide, and parachute descent, all of the three individual fatality values are summed up to obtain the total risk of flying within the designated cell.

$$P_{\text{fatality}} = P_{\text{fatality, outside}} + P_{\text{fatality, inside}} \tag{15}$$

4 Application to minimum risk path planning

A visual analysis of GRMs gives already fundamental insights how people and buildings on the ground influence the availability of urban airspace. This could enable for example the identification of high risk zones that operators might avoid. A more sophisticated exploitation of the GRMs, however, is the application for flight route planning using path planning algorithms. Graph-based algorithms like the famous A* algorithm can use cost maps to find a cost-optimal solution between a pair of Origin and Destination coordinates (OD pair). The GRMs can be interpreted directly as such cost maps. Therefore, they can be used in combination with an optimal path planning algorithm to determine the minimum risk path between any OD pair within the boundaries of the GRM. Since the underlying grid of the map is in the Mollweide projection, the path lengths have to be transformed to that projections as well. This is important because the cost of movement from one cell to another is defined by a linear combination of the risk and the length of the exposure as recommended by Sedov et al. [23]. This way, the calculated path has the lowest accumulated risk over the total mission path. However, for the comparison of different risk paths the median risk is considered. This introduces robustness against outliers when compensating high-risk zones with zones of lower risk, accounting for the fact that all risk values are afflicted by uncertainties. The heuristic is defined as the minimum risk value of the entire map not equal to zero, which prevents the algorithm from losing track in large areas of zero risk. While this heuristic may overestimate the cost in the latter case (prioritizing performance over accuracy), it is guaranteed to find an optimal path if there are no zero-risk areas on the map. Finally, the calculated flight paths are smoothed using a B-spline interpolation. If not stated otherwise, the GRMs reported in the following are calculated with the parameters shown in Table 5. Figure 8 presents the GRM and the minimum risk path of the Paris scenario. The large, noticeable area of high risk over the city is caused by the very high population density in Paris. The minimum risk path still crosses a part of this high risk area showcasing the target of the path planning algorithm to minimize the globally accumulated risk. Taking a detour could avoid passing areas of particular high risk but the longer exposure over other areas cancels out the advantage.

Table 5: Input parameters of the reference mission

Input parameter	**Value**	**Input parameter**	**Value**
Mission parameters		**Vehicle specifications**	
Day of the mission	Weekday	eVTOL type	L+C PS
Daytime (24h format)	09:00	Horizontal speed [$\mathrm{m\,s^{-1}}$]	N(57,2)
Height AGL [m]	N(1000,10)	Vertical speed [$\mathrm{m\,s^{-1}}$]	N(0,2)
Weather		Heading [°] (min,max)	(180,270)
Wind speed [$\mathrm{m\,s^{-1}}$]	N(5,3)	Density of fuselage material [$\mathrm{g\,cm^{-2}}$]	2.7
Wind direction [°]	N(220,30)	Flow stress of fuselage [MPa]	350
Impact characteristics		**Calculation parameters**	
Flow stress of building shell [MPa]	N(300,50)	Simulation runs per cell	1000
AIS_{max}	2		

Figure 9 shows the minimum risk paths at day time and at night time for the Seoul scenario. The flight path at night is $14\,\%$ shorter. The median risk with 0.25×10^{-6} fatalities per flight hour is an order of magnitude higher at day time than during night time (0.49×10^{-7} fatalities per flight hour).

5 Discussion

The presented GRMs enable the calculation of minimum risk paths for UAM operations. As expected, the population density has a high influence on the GRMs which can be seen when comparing results at day time and night time. The introduction of a dynamic population distribution model revealed that the higher population density

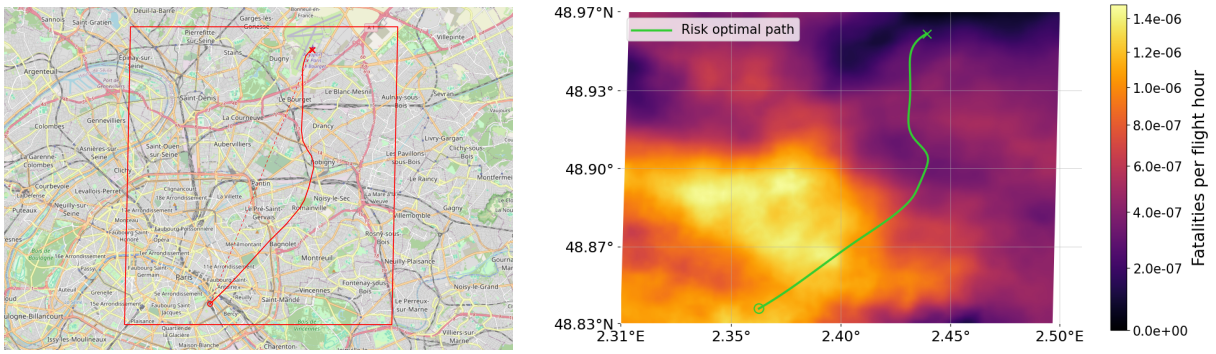

(a) Reference map

(b) Ground risk map

Figure 8: Ground risk map and minimum risk path in Paris, mission parameters as reported in Table 5.

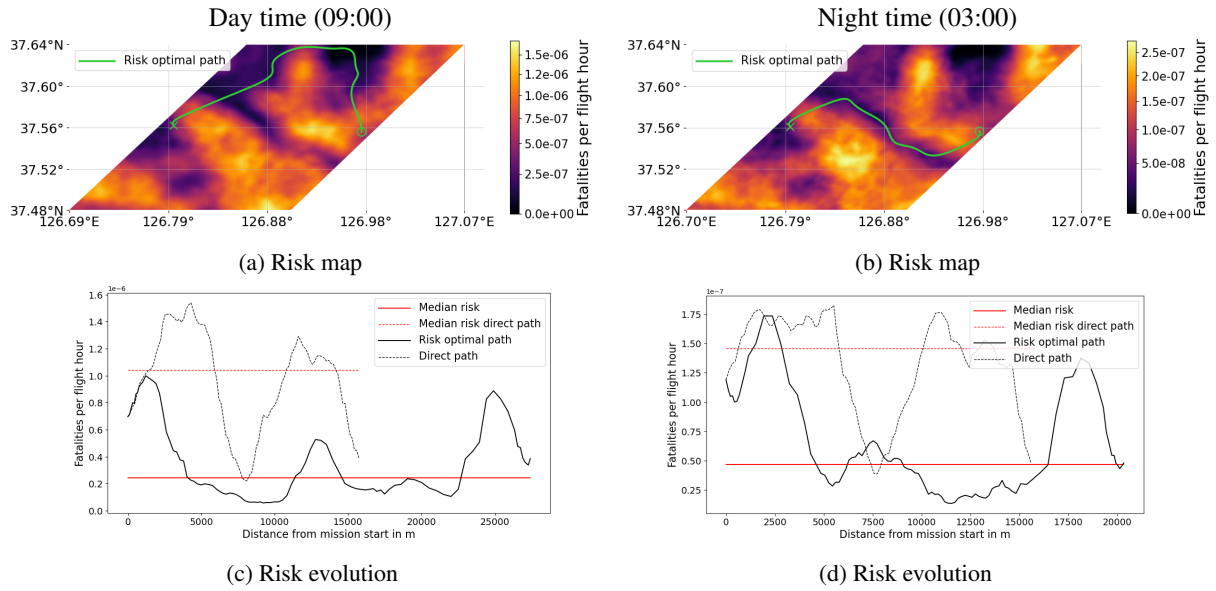

(a) Risk map

(b) Risk map

(c) Risk evolution

(d) Risk evolution

Figure 9: Investigation of the influence of the time of day on the minimum risk path at the example of Seoul. The minimum risk path at night time is shorter.

outside during the day increases the ground risk. The usage of the NRES classification and the built-up surface area as metrics for the redistribution are considered as an acceptable trade-off between generalization and accuracy of the population model. First attempts from literature to assess the population distribution using cell phone data did not produce reliable results with a higher resolution than the data provided in the GHSL [1], [10]. The current population model could be extended by a representation of large gatherings of people (e.g. demonstrations) and seasonal differences.

The aircraft failure model introduced in this work aims to capture the uncertainties related to an eVTOL crash. At each point, the direction of the uncontrolled descent is assumed to be uniformly probable in all directions. This is necessary because during GRM calculation, the flight direction is unknown. In reality, an eVTOL would likely descend in the direction of its initial horizontal velocity. A potential solution could be to set fixed flight directions for a set of flight segments. For each segment, the descent trajectories could then be modelled in a more narrow interval. The magnitude of the risk is sensitive to the failure rates that are used in the calculations. The assumption of failure rates for aircraft in this work are necessary due to the lack of experimental or historical data and should be replaced once this data is available.

The impact model finally provides more details with regard to the interaction between aircraft and buildings then the existing literature for GRMs. Nevertheless, the different structural mechanics of different building materials could be captured in the future. Knock-on effects after the first impact of an descending aircraft with any ground structure include the collapse of buildings and fire outbreaks. Their consequences could be much worse than the direct impact of the kinetic energy of the eVTOL, albeit hard to predict.

6 Conclusion

In this paper, a novel risk assessment for eVTOL operations in the context of UAM is proposed. The risk assessment calculates the fatalities potentially caused by an eVTOL based on the probabilities for an uncontrolled descent. Consideration of different descent trajectories allow the prediction of the impact point on the ground. The impact model is based on a dynamic population model and data on building density. In addition, the impact severity is modelled differently depending on the position of the impacted people in- or outside. This enables to calculate the sheltering factor of buildings by estimating the dissipated kinetic energy. Implementation of the risk assessment methodology leads to the generation of ground risk maps. These maps are used to calculate minimum risk paths. Although this application is only a starting point, the results show that the proposed approach can avoid high risk areas for the cost of additional flight distance. Future work will include research of path planning techniques that find an optimal trade-off between induced ground risk and other optimisation goals such as the consumed energy.

References

[1] Christa Brelsford, Jessica Moehl, Eric Weber, Kevin Sparks, Joseph V. Tuccillo, and Amy Rose. Spatial and temporal characterization of activity in public space. *Scientific Data*, 9, 2022.

[2] Cirrus Owners & Pilots Association. Caps event history, 2024.

[3] Victor R. Clare, James H. Lewis, Alexander P. Mickiewicz, and Larry M. Sturdivan. Blunt trauma data correlation.

[4] DIN German Institute for Standardization. Din 33402-2, ergonomie – körpermaße des menschen – teil 2: Werte, 2020.

[5] Mo Elsayed and Moataz Mohamed. The impact of airspace regulations on unmanned aerial vehicles in last-mile operation. *Transportation Research Part D: Transport and Environment*, 87:102480, 2020.

[6] European Union Aviation Safety Agency. Study on the societal acceptance of urban air mobility in europe, 2021.

[7] Sergio Freire, Kytt MacManus, Martino Pesaresi, Erin Doxsey-Whitfield, and Jane Mills. Development of new open and free multi-temporal global population grids at 250 m resolution. geospatial data in a changing world. In Association of Geographic Information Laboratories in Europe, editor, *19th AGILE*, 2016.

[8] Laurie A. Garrow, Brian J. German, and Caroline E. Leonard. Urban air mobility: A comprehensive review and comparative analysis with autonomous and electric ground transportation for informing future research. *Transportation Research Part C: Emerging Technologies*, 132:103377, 2021.

[9] Matt Grote, Aliaksei Pilko, James Scanlan, Tom Cherrett, Janet Dickinson, Angela Smith, Andrew Oakey, and Greg Marsden. Sharing airspace with uncrewed aerial vehicles (uavs): Views of the general aviation (ga) community. *Journal of Air Transport Management*, 102:102218, 2022.

[10] Sandra Hadam, Timo Schmid, and Joanna Simm. Kleinräumige prädiktion von bevölkerungszahlen basierend auf mobilfunkdaten aus deutschland. In Bettina Klumpe, Jette Schröder, and Markus Zwick, editors, *Qualität bei zusammengeführten Daten*. Springer Fachmedien Wiesbaden, Wiesbaden, 2020.

[11] Neil Edward Klepeis, William C. Nelson, Wayne Ott, and John P. Robinson. The national human activity pattern survay (nhaps): a resource for assessing exposure to environmental pollutants. *Journal of Exposure Science & Environmental Epidemiology*, 11, 2001.

[12] Anders La Cour-Harbo. Quantifying ground impact fatality rate for small unmanned aircraft. *Journal of Intelligent & Robotic Systems*, 93, 2019.

[13] Anders La Cour-Harbo. Ground impact probability distribution for small unmanned aircraft in ballistic descent. In ICUAS, editor, *International Conference on Unmanned Aircraft Systems*, 2020.

[14] Christopher Lum and Blake Waggoner. A risk based paradigm and model for unmanned aerial systems in the national airspace. In *Infotech@Aerospace 2011*, Reston, Virigina, 2011. American Institute of Aeronautics and Astronautics.

[15] Robert C. Matthews, Rex Alexander, and Richard B. Stone. Helicopter accident trends in 8 isasi countries and how we might improve the fatal accident even further, 2015.

[16] Mark Wilfried Müller. *Increased autonomy for quadrocopter systems: trajectory generation, fail-safe strategies and state estimation*. Dissertation, ETH Zurich, 2016.

[17] Michael D. Patterson, Lee W. Kohlman, and Kevin Antcliff. A proposed approach to studying urban air mobility missions including an initial exploration of mission requirements. In Vertical Flight Society, editor, *74th Annual American Helicopter Society International Forum and Technology Display 2018 (FORUM 74)*, 2018.

[18] Martino Pesaresi, Christina Corbane, Chao Ren, and Ng Edward. Generalized vertical components of built-up areas from global digital elevation models by multi-scale linear regression modelling. *Plos One*, 16, 2021.

[19] Martino Pesaresi and Panagiotis Politis. Ghs-built-v r2023a - ghs built-up volume grids derived from joint assessment of sentinel2, landsat, and global dem data, multitemporal (1975-2030), 2023.

[20] Stefano Primatesta, Alessandro Rizzo, and Anders La Cour-Harbo. Ground risk map for unmanned aircraft in urban environments. *Journal of Intelligent & Robotic Systems*, 97(3-4):489–509, 2020.

[21] Jorge D. Riera. On the stress analysis of structures subjected to aircraft impact forces. *Nuclear Engineering and Design*, 8:415–426, 1968.

[22] M. Schiavina, S. Freire, A. Carioli, and K. MacManus. Ghs-pop r2023a - ghs population grid multitemporal (1975-2030), 2023.

[23] Leonid Sedov, Valentin Polishchuk, and Bulusu Vishwanath. Ground risk vs. efficiency in urban drone operations. In ATM Seminar, editor, *AA/Europe ATM R&D Seminar 2021*, 2021.

[24] Christopher Silva, Wayne Johnson, Kevin R. Antcliff, and Michael D. Patterson. Vtol urban air mobility concept vehicles for technology development. In American Institute of Aeronautics and Astronautics, editor, *Aviation Technology, Integration, and Operations Conference*, 2018.

[25] Jakub Slama, Petr Vana, and Jan Faigl, editors. *Risk-aware Trajectory Planning in Urban Environments with Safe Emergency Landing Guarantee*, 2021.

[26] John P. Snyder. Map projections: A working manual, 1987.

[27] Christian Stein. Neue datenquellen zur beruflichen mobilität. das beispiel frankfurt am main. *Zeitschrift des Verbandes Deutscher Städtestatistiker*, 1, 2020.

[28] Anna Straubinger, Raoul Rothfeld, Michael Shamiyeh, Kai-Daniel Büchter, Jochen Kaiser, and Kay Olaf Plötner. An overview of current research and developments in urban air mobility – setting the scene for uam introduction. *Journal of Air Transport Management*, 87, 2020.

[29] Tourismus+Congress GmbH Frankfurt am Main. Gäste- und übernachtungszahlen 2022: Offizielle statistische auswertung für die stadt frankfurt am main, 2023.

[30] Darli Rodrigues Vieira, Dreyfus Silva, and Alencar Bravo. Electric vtol aircraft: the future of urban air mobility (background, advantages and challenges). *International Journal of Sustainable Aviation*, 5(2):101, 2019.

[31] Tomasz Wierzbicki, Liang Xue, and Meg Hendry-Brogan. Aircraft impact damage. In Eduardo Kausel, editor, *The Towers Lost and Beyond*. 2002.

[32] Pengcheng Wu, Junfei Xie, Yanchao Liu, and Jun Chen. Risk-bounded and fairness-aware path planning for urban air mobility operations under uncertainty. *Aerospace Science and Technology*, 127:107738, 2022.